Journal of Ethnopharmacology 267 (2021) 113605

Contents lists available at ScienceDirect

Journal of Ethnopharmacology

journal homepage: www.elsevier.com/locate/jethpharm

22β-hydroxytingenone induces apoptosis and suppresses invasiveness of melanoma cells by inhibiting MMP-9 activity and MAPK signaling

Elenn Suzany Pereira Aranha [a], Adrhyann Jullyanne de Sousa Portilho [f], Leilane Bentes de Sousa [d], Emerson Lucena da Silva [f], Felipe Pantoja Mesquita [f], Waldireny C. Rocha [c], Felipe Moura Araújo da Silva [b], Emerson Silva Lima [d], Ana Paula Negreiros Nunes Alves [f], Hector Henrique Ferreira Koolen [e], Raquel Carvalho Montenegro [f], Marne Carvalho de Vasconcellos [d,*]

[a] Faculty of Pharmaceutical Sciences, Post Graduate Program in Biodiversity and Biotechnology of the Amazon (Bionorte), Federal University of Amazonas, Manaus, Amazonas, 69080-900, Brazil
[b] Department of Chemistry, Federal University of Amazonas, Manaus, Amazonas, 69080-900, Brazil
[c] Health and Biotechnology Institute, Federal University of Amazonas, Coari, Amazonas, 69460-000, Brazil
[d] Faculty of Pharmaceutical Sciences, Federal University of Amazonas, Manaus, Amazonas, 69080-900, Brazil
[e] Metabolomics and Mass Spectrometry Research Group, Amazonas State University (UEA), Manaus, Amazonas, 690065-130, Brazil
[f] Drug Research and Development Center (NPDM), Federal University of Ceará, Fortaleza, Ceará, 60430-275, Brazil

ARTICLE INFO

Keywords:
SK-MEL-28
Apoptosis
Invasion
Quinonemethide triterpenes

ABSTRACT

Ethnopharmacological relevance: 22β-hydroxytingenone (22-HTG) is a quinonemethide triterpene isolated from *Salacia impressifolia* (Miers) A. C. Smith (family Celastraceae), which has been used in traditional medicine to treat a variety of diseases, including dengue, renal infections, rheumatism and cancer. However, the anticancer effects of 22-HTG and the underlying molecular mechanisms in melanoma cells have not yet been elucidated.
Aim of the study: The present study investigated apoptosis induction and antimetastatic potencial of 22-HTG in SK-MEL-28 human melanoma cells.
Materials and methods: First, the *in vitro* cytotoxic activity of 22-HTG in cultured cancer cells was evaluated. Then, cell viability was determined using the trypan blue assay in melanoma cells (SK-MEL-28), which was followed by cell cycle, annexin V-FITC/propidium iodide assays (Annexin/PI), as well as assays to evaluate mitochondrial membrane potential, production of reactive oxygen species (ROS) using flow cytometry. Fluorescence microscopy using acridine orange/ethidium bromide (AO/BE) staining was also performed. RT-qPCR was carried out to evaluate the expression of *BRAF, NRAS,* and *KRAS* genes. The anti-invasiveness potential of 22-HTG was evaluated in a three-dimensional (3D) model of reconstructed human skin.
Results: 22-HTG reduced viability of SK-MEL-28 cells and caused morphological changes, as cell shrinkage, chromatin condensation, and nuclear fragmentation. Furthermore, 22-HTG caused apoptosis, which was demonstrated by increased staining with AO/BE and Annexin/PI. The apoptosis may have been caused by mitochondrial instability without the involvement of ROS production. The expression of *BRAF*, *NRAS*, and *KRAS*, which are important biomarkers in melanoma development, was reduced by the 22-HTG treatment. In the reconstructed skin model, 22-HTG was able to decrease the invasion capacity of melanoma cells in the dermis.

Abbreviations: 22-HTG, 22β-hydroxytingenone; MAPK, mitogen-activated protein kinase; DMSO, dimethyl sulfoxide; SK-MEL-28, human melanoma cells; MES-SA/DX, human doxorubicin resistant uterine sarcoma cells; DU 145, human prostate cancer cell line; MRC-5, normal cell derived from human pulmonary fibroblast; DMEM, Dulbecco's Modified Eagle's Medium; IC_{50}, 50% inhibitory concentration; PI, propidium iodide; AO, acridine orange; EB, ethidium bromide; DCFH-DA, 2′,7′-Dichlorodihydrofluorescein diacetate; qRT-PCR, quantitative real-time PCR; ACTB, actin beta; 3D, three-dimensional; ROS, reactive oxygen species; PBS, phosphate buffered saline.

* Corresponding author.Faculdade de Ciências Farmacêuticas, Universidade Federal do Amazonas, Av. General Octávio Jordão Ramos, 3000, Japiim, CEP 69080-900, Manaus, Amazonas, Brazil.

E-mail addresses: elenn_suzany@yahoo.com.br (E.S.P. Aranha), dryportilhoo@gmail.com (A.J.S. Portilho), leilane.bentes@gmail.com (L. Bentes de Sousa), lucenaemerson@hotmail.com (E.L. da Silva), felipe_mesquita05@hotmail.com (F.P. Mesquita), wal2002@gmail.com (W.C. Rocha), felipesaquarema@bol.com.br (F.M. Araújo da Silva), eslima75@gmail.com (E.S. Lima), ananegreirosnunes@gmail.com (A.P.N.N. Alves), hectorkoolen@gmail.com (H.H.F. Koolen), rcm.montenegro@gmail.com (R.C. Montenegro), marnevasconcellos@yahoo.com.br (M.C. Vasconcellos).

https://doi.org/10.1016/j.jep.2020.113605
Received 29 September 2020; Received in revised form 11 November 2020; Accepted 17 November 2020
Available online 21 November 2020

Conclusions: Our data indicate that 22-HTG has anti-tumorigenic properties against melanoma cells through the induction of cell cycle arrest, apoptosis and inhibition of invasiveness potential, as observed in the 3D model. As such, the results provide new insights for future work on the utilization of 22-HTG in malignant melanoma treatment.

1. Introduction

The liana *Salacia impressifolia* (Miers) A. C. Smith is distributed from Central to South America, and is particularly common in the Amazon Rainforest (Lombardi, 2010). In the North of Brazil, *S. impressifolia* is popularly known as "miraruíra" or "cipó-miraruíra", which is also the popular name for Amazonian *Connarus* spp. and, through stem decoction, both are used to treat inflammations and diabetes (Lorenzi and Matos, 2002). In the Peruvian Amazon, *S. impressifolia* is popularly known as "panu" and is used in various treatments, such as for dengue, renal affections, rheumatism and cancer (Brako and Zarucchi, 1993; Clavo et al., 2003).

Rodrigues et al. (2019) reported the cytotoxic activity of the extract and fraction of *S. impressifolia* against different cell lines. The authors demonstrated anticancer potential *in vitro* and *in vivo* and observed the presence of quinonemethide triterpenoids, in particular, the compounds tingenone and 22β-hydroxytingenone (22-HTG). Notably, the results obtained against the SK-MEL-28 cell line (human melanoma cells) (Aranha et al., 2020) with 22-HTG have encouraged more studies to evaluate its mechanism of action. Among types of skin cancer, melanoma is the most aggressive and lethal form of tumor (Leonardi et al., 2018) and it is the type of cancer most associated with genetic changes, which lead to uncontrolled cell proliferation and the appearance of an invasive cell phenotype (Savoia et al., 2019).

Mutations in the oncogenes *BRAF* and *NRAS* are reported in patients with melanoma, and the dysregulation in these genes can lead to alterations in some cell signaling pathways, such as mitogen-activated protein kinase (MAPK), also known as RAS/RAF/MEK/ERK. The loss of control of signaling processes in the MAPK pathway can lead to uncontrolled cell proliferation, invasion, metastasis, survival, angiogenesis, and apoptosis inhibition, which are involved in melanoma development (Moreira et al., 2020).

Prognosis of patients with early-stage melanoma has improved in recent years with the advances in the development of targeted therapies using specific inhibitors and immunotherapies (Berning et al., 2019). Despite the important progress of these therapies and the advancements that have been made in the clinical treatment of melanoma, there is still a significant risk of drug resistance or overstimulation of the immune system, which, in the long-term, can lead to a poor prognosis (Berning et al., 2019; Kozar et al., 2019). For this reason, there is a need to identify new alternative therapies that are capable of affecting molecular events and enhancing the quality of life of patients with melanoma (Menezes et al., 2018).

Natural products are a promising source of anti-melanoma compounds (Huang et al., 2020), which may even be used in combination with existing therapy to enhance the pharmacological effect and reduce toxicity (Oprean et al., 2018). Therefore, this work aimed the study of the biological activity of 22-HTG, along with with the evaluation of apoptosis induction and reduction of invasiveness potentials, along with an investigation of the molecular mechanism associated to these effects.

2. Materials and methods

2.1. Extraction and isolation of 22β-hydroxytingenone

Stems and leaf stalks of *S. impressifolia* (Miers) A. C. Smith (Celastraceae) were collected at Adolpho Ducke Reserve (coordinates 2°56′58.2'' S, 59°56′36.3'' W) located in the municipality of Manaus, Amazonas state, Brazil. A specimen voucher (#4699) was deposited in the herbarium of the National Institute for Amazonian Research (INPA), Brazil. The access was registered (number: A715C2F) in SisGen-Brazilian National System of Genetic Resource Management and Associated Traditional Knowledge, and complied with their guidelines. The plant extraction, isolation workflow, structural confirmation, and purity of the 22β-hydroxytingenone (22-HTG) were as previously described (Aranha et al., 2020; da Silva et al., 2016). For all experiments *in vitro*, 22-HTG (Fig. 1) was dissolved in dimethyl sulfoxide (DMSO) and diluted with culture medium so that the final concentration in the cell cultures did not exceed 0.2% DMSO (v/v).

2.2. Cell line and culture conditions

Human melanoma cells (SK-MEL-28), human doxorubicin resistant uterine sarcoma cells (MES-SA/DX), human prostate cancer cell line (DU 145), human epidermal keratinocytes (HaCat), and the normal cell derived from human pulmonary fibroblast (MRC-5) were utilized in this study. Cells were grown in 75 cm^2 culture flasks, containing Dulbecco's Modified Eagle's Medium (DMEM, Gibco™ #12100046), supplemented with 10% bovine fetal serum (FBS, Gibco™ #12657029) and 1.0% penicillin-streptomycin (Pen Strep, Gibco™ #15070063), and maintained at 37 °C in a 5% humidified atmosphere. At 90% confluence, the cells were harvested using 0.05% Trypsin-EDTA (Gibco™ #25300062) and seeded in 96, 12 or 24-well plates according to the type of experiment being performed. For all the tests, cells were allowed to adhere to the surface prior to treatment.

2.3. Cell viability assay

The 50% inhibitory concentration (IC_{50}) was determined using an Alamar blue assay (resazurin 7-Hydroxy-3*H*-phenoxazin-3-one-10-oxide) (Ansar Ahmed et al., 1994). For the assay, SK-MEL-28, MES-SA/DX, DU 145, and MRC-5 were plated (0.5×10^4/well) in a 96-well plate and exposed to different concentrations (20 – 0.625 μM) of 22-HTG for period of 72 h. After the treatment, 10 μL of 0.02% Alamar blue solution in DMEM were added to each well. Fluorescence was measured by using 465 nm excitation and 540 nm emission in a microplate reader (DTX 800 Beckman Coulter Multimode Detector). This assay was used to determine the cell line and concentrations used in subsequent tests.

Cell viability was assessed by trypan blue exclusion assay (Strober, 2001). SK-MEL-28 cells (0.3×10^5 cells/well) were plated in 12-well plates and after adhesion were exposed to 22-HTG (2.5 and 5.0 μM) for 24 h. Subsequently, cells were harvested and, in order to estimate cellular viability, trypan blue solution (0.4%) was used in a hemocytometer chamber to differentiate living and dead cells under microscopy (Carl ZTMeiss Microscopy GmbH/Axiocam ERc 5s).

2.4. Analysis of cell morphology

SK-MEL-28 cells (0.5×10^5 cells/well) were plated in 24-well plates and allowed to adhere. Next, cells were treated with 22-HTG (2.5 and 5.0 μM) for 24 h. After treatment, cells were resuspended in the culture medium and slides were made using cytocentrifugation (450 g/5 min). Cells were fixed and stained with a LaborClin® rapid panoptic dye kit. The cells were analyzed and morphological changes in the cytoplasm and nucleus were photographed using light microscopy (Eclipse Ni–U-Nikon).

2.5. Cell cycle analysis

The potential of the 22-HTG to interfere with the cell cycle of SK-MEL-28 human melanoma cells was evaluated using flow cytometry with propidium iodide (PI) as a cell marker (Vartholomatos et al., 2015). SK-MEL-28 cells (0.5 x 10^5 cells/well) were plated in 24-well plates and allowed to adhere. After, cells were treated with 22-HTG (2.5 and 5.0 μM) for 24 h. Subsequently, cells were harvested, centrifuged at 247 g for 5 min at 4°C, and the cell pellet was fixed using 70% cold ethanol overnight. Afterwards, cells were centrifuged under the same conditions as the previous step. The supernatant was removed and the cells were stained with 100 μL PI solution (5 μg/mL) for 30 min at 4 °C. The fluorescent emission was measured in a flow cytometer (FACSCanto II, BD Biosciences, OR, USA).

2.6. Acridine orange and ethidium bromide cell staining

Acridine orange (AO) and ethidium bromide (EB) staining were used to distinguish viable from apoptotic and necrotic cells (Ralph et al., 2016). SK-MEL-28 cells (0.3 x 10^5 cells/well) were plated in 24-well plates and allowed to adhere. Next, cells were treated with 22-HTG (2.5 and 5.0 μM) for 24 h. After the period of exposure to the substance, cells were harvested, centrifuged at 247 g for 5 min at 4 °C, resuspended in 30 μL of culture medium and stained with 2 μL of an aqueous solution AO/EB (100 μg/mL; AO/EB). The cell suspension was immediately examined using fluorescence microscopy (Eclipse Ni–U-Nikon). Images obtained were then analyzed and cell percentage was quantified as either viable (uniform bright green nuclei with an organized structure), apoptotic (orange to red nuclei with condensed to fragmented chromatin and green cytoplasm) or necrotic cells (uniformly orange to red nuclei with an organized structure and red cytoplasm).

2.7. Apoptosis assay

Apoptosis was evaluated by double-labeled flow cytometry analysis with Annexin V-FITC and PI, which permits the detection of apoptotic and necrotic cells due to modifications in the plasmatic membrane (Guerra et al., 2017). SK-MEL-28 cells (0.3 x 10^5 cells/well) were plated in 24-well plates and allowed to adhere. After, cells were treated with 22-HTG (2.5 and 5.0 μM) for 24 h. Subsequently, the cells were harvested and centrifuged at 247 g for 5 min at 4 °C. The cell pellet was stained with 5 μL of Annexin V-FITC and 5 μL of PI solution and left for 15 min at room temperature (25 °C), in the dark, as recommended by FITC Annexin V Apoptosis Detection Kit I (BD Pharmingen™). Finally, the fluorescence was evaluated using flow cytometry (FACSCanto II, BD Biosciences, OR, USA).

2.8. Evaluation of mitochondrial membrane potential

The evaluation of the mitochondrial membrane potential was performed to investigate the effect of 22-HTG on mitochondrial metabolism byusing fluorescent labeling with rhodamine 123 (Amaral-Machado et al., 2019). SK-MEL-28 cells (0.3 x 10^5 cells/well) were plated in 12-well plates and allowed to adhere. After, cells were treated with 22-HTG (2.5 and 5.0 μM) for 24 h. Next, cells were harvested, centrifuged at 247 g for 5 min at 4 °C, and cell pellets were resuspended in rhodamine 123 solution (5 μg/mL) for 30 min at 37°C and maintained in a 5% CO_2 atmosphere, in the dark. Then, the mitochondrial membrane potential was evaluated using flow cytometry (FACSCanto II, BD Biosciences, OR, USA).

2.9. Evaluation of intracellular reactive oxygen species (ROS) levels

2′,7′-Dichlorodihydrofluorescein diacetate (DCFH-DA) fluorescent

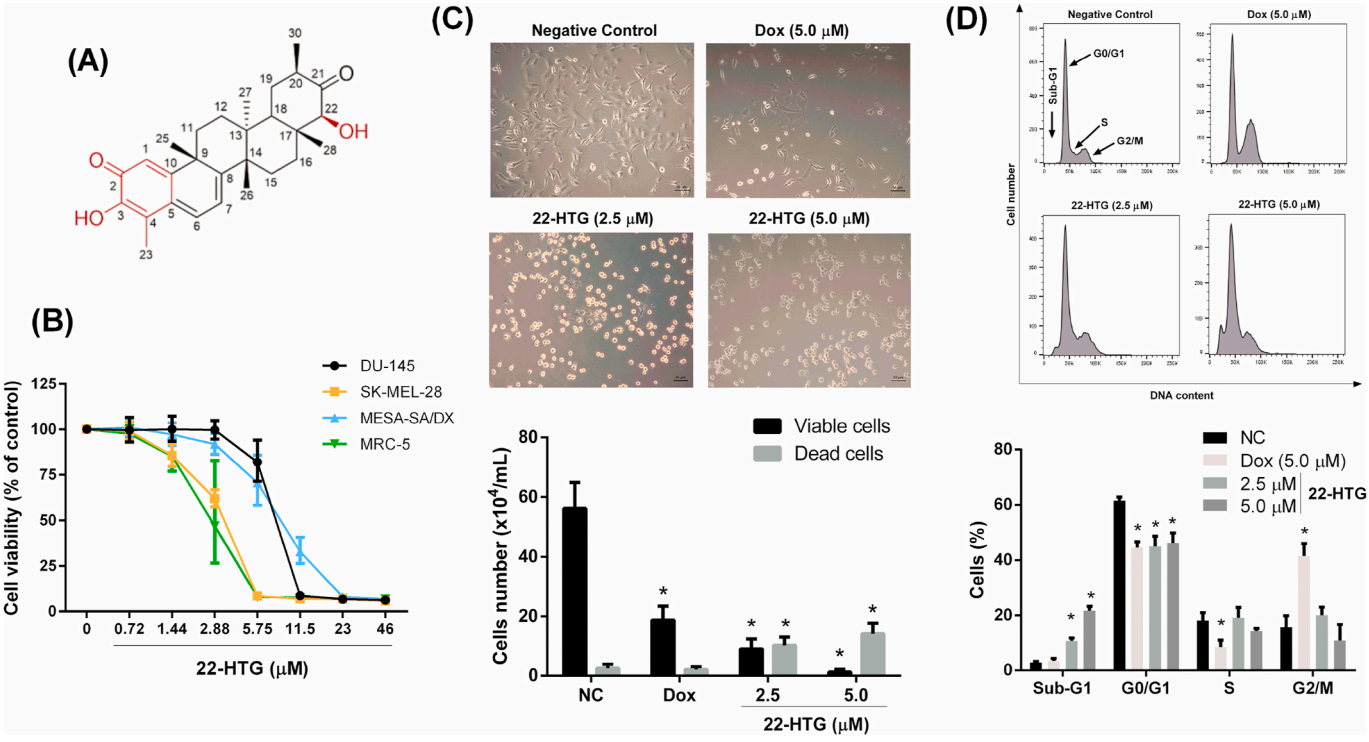

Fig. 1. Inhibition of cell proliferation by treatment with 22β-hydroxytingenone (22-HTG). (A) Chemical structure of 22-HTG. (B) Cell survival curves obtained using Alamar blue assay after 72 h of incubation. Cancer cells: human prostate cancer cell line (DU 145); human malignant melanoma (SK-MEL-28); human doxorubicin-resistant uterine sarcoma cells (MES-SA/DX). Noncancerous cells: MRC- 5 (human lung fibroblast). (C) Effect of 22-HTG on cell viability of SK-MEL-28 cells after 24 h of exposure. (D) Cell cycle distribution in SK-MEL-28 cells after 24 h treatment with 22-HTG. The images and values represent results from three independent experiments, mean ± SD. *$p < 0.05$ was considered significant when compared to the negative control (NC). Dox- Doxorubicin (5.0 μM) was used as the positive control. (For interpretation of the references to colour in this figure legend, the reader is referred to the Web version of this article.)

dye was used to determine the intracellular ROS levels of the SK-MEL-28 cell line (Ribeiro et al., 2018). SK-MEL-28 cells (0.3 x 10^5 cells/well) were plated in 12-well plates and allowed to adhere. After, cells were treated with 22-HTG (2.5 and 5.0 μM) for 3 h. Subsequently, the cells were incubated with DCFH-DA solution (10 μM) for 30 min at 37 °C and maintained in a 5% CO_2 atmosphere. Afterwards, the cells were washed twice with PBS, harvested, and centrifuged at 247 g for 5 min at 4 °C. Cell pellets were resuspended with 400 μL of PBS and the intracellular ROS levels were determined using flow cytometry (FACSCanto II, BD Biosciences, OR, USA).

2.10. Total mRNA isolation and expression analysis by qRT-PCR

The effects of 22-HTG on the mRNA expression *BRAF, NRAS*, and *KRAS* were analyzed. SK-MEL-28 cells (0.4 x 10^5 cells/well) were seeded in 24-well plates and allowed to adhere. After, cells were treated with 22-HTG (2.5 μM) for 24 h. TRIzol® Reagent (Life Technologies, USA) was used for total RNA extraction. PCR primer sequences of each gene were designed using OligoPerfect Designer (Invitrogen), and are described in Table 1. Expression levels of *BRAF*, *NRAS*, and *KRAS* were determined in triplicate using the stable expressed Actin Beta (ACTB) gene as the endogenous control. Quantitative reverse transcriptase-PCR (qRT-PCR) reactions were performed as described previously (Aranha et al., 2020). Minimum Information for Publication of Quantitative Real-Time PCR Experiments - MIQE Guidelines were followed (Bustin et al., 2009), and the expression level was calculated using the $2^{-\Delta\Delta CT}$ method (Schmittgen and Livak, 2008), considering negative control samples as the calibrator of the experiments.

2.11. Artificial skin reconstruction

The human skin equivalent was reconstructed in two steps according to Boelsma et al. (2000); Maria and Wada (1997); Pedrosa et al. (2017), with modifications. First, MRC5 cells (25 x 10^4 cells/skin) were gently mixed with 700 μL of collagen type I (2.3 mg/mL, A10483-01 Gibco™), 108 μL of reconstruction buffer 10X (NaOH 0.05 M, $NaHCO_3$ 2.2%, HEPES 200 mM), and 108 μL of Ham's F12 Nutrient Mixture 10X. After gently mixing gel solution with MRC5, 800 μL/insert this solution was quickly transferred to a Corning 12 mm Transwell® with a 0.4 μm pore polyester membrane plate insert using a 12-well plate. After polymerization of the collagen gel, a collagen type IV (6 μg/mL – C7521 SIGMA) coating was performed on the matrix with fibroblasts. The supplemented DMEM/F12 medium was added to the well in the plate, and was then incubated at 37 °C for 1 h for pH adjustment. For next step, HaCat (50 x 10^4 cells/skin) and SK-MEL-28 (25 x 10^4 cells/skin) cells were mixed and seeded on the surface of a collagen gel to grow to full thickness skin, and then were kept submerged in for 24 h, which was followed by 10 days at the air-liquid interface. The supplemented DMEM/F12 medium was changed every two days up until 10 days. Subsequently, the reconstructed skin was treated with 5.0 μM of 22-HTG for 72 h, followed by fixation with 10% buffered formaldehyde at 4 °C, then dehydrated with alcohol, and embedded in paraffin. For morphological analyses, the samples were stained with hematoxylin and eosin.

Table 1
Sequence of oligonucleotides used for qRT-PCR.

Gene	Sequence (5'- 3')	NCBI reference sequence
BRAF	F- CATCCACAGAGACCTCAAGAGT R- ATGACTTCTGGTGCCATCC	NM_001354609.2
NRAS	F- TCCAGCTAATCCAGAACCAC R- TTCGCCTGTCCTCATGTATT	NM_002524.5
KRAS	F- TTGTGGTAGTTGGAGCTGGT R- ACTCCTCTTGACCTGGTGTG	NM_001369787.1
ACTB[a]	F- CTGGAACGGTGAAGGTGACA R- AAGGGACTTCCTGTAACAACGCA	NM_001101.5

[a] Actin Beta (ACTB) gene was used as the endogenous control.

2.12. Determination of MMP activity using gelatin zymography

MMP-2 and MMP-9 activity in conditioned organotypic media was determined using gelatin zymography. In the final experiments, the media were collected and centrifugated at 425 x *g* for 10 min at 4 °C to remove cell debris. Total protein contents were normalized using the Bradford protein determination method. The cell-conditioned medium was subjected to substrate-gel electrophoresis. A similar amount of protein containing the conditioned media was applied to 10% polyacrylamide gels containing 1.0 mg/mL gelatin. After electrophoresis, polyacrylamide gels were washed with 2.5% Triton X-100 at room temperature to remove the sodium dodecyl sulfate. Gels were then incubated overnight at 37 °C in a buffer containing 5.0 mM $CaCl_2$, 50 mM Tris–HCl pH 8.5 and 5.0 μM $ZnCl_2$ for the MMP to digest the gelatin. The gels were stained with 1% Brilliant Blue R in 45% methanol and 10% glacial acetic acid. After 30 min, the gels were destained in the same solution without the Coomassie blue dye. Proteolytic activity was detected as clear zones against the background stain of undigested substrate. Then, the intensities of the bands were estimated using ImageJ Software®.

2.13. Statistical analysis

All data were presented as the mean ± standard deviation (SD) from three independent experiments performed in triplicate. Cell viability was expressed as IC_{50} and was obtained using nonlinear regressions based on three replicates per concentration. Statistical differences ($p < 0.05$) were obtained by comparison with the negative control (DMSO 0.2%) using analysis of variance (ANOVA), followed by Tukey's or Bonferroni's post-test on GraphPad Prism 6.0 for Windows (Graphpad, San Diego, CA).

3. Results

3.1. 22-HTG induces reductions in cell viability in SK-MEL-28 cells

Fig. 1-(B) presents the cell survival curves obtained after treatment with 22-HTG. We evaluated the effect of 22-HTG in cancer cell lines derived from the prostate (DU 145), uterus (multidrug-resistant) (MES-SA/DX), and melanoma (SK-MEL-28). These cell lines were choice for screening cytotoxic because represent common human solid tumor malignancies with propriety of aggressiveness, metastasis and resistance (Daveri et al., 2015; Greer and Ivey, 2007; Rosenberg et al., 2014).

The concentrations of the compound that reduced cell growth by 50% (IC_{50} values) are shown in Table 2. From the comparison of the activity toward cell lines, we shown that 22-HTG was active against SK-MEL-28 and DU-145, and simultaneously possess comparable cytotoxicity against the doxorubicin resistant MES-SA/DX cell line. This effect is promising, because it shows the ability to overcome the multidrug resistance of MES-SA/DX cell line, suggesting that 22-HTG may

Table 2
C_{50} values on cancer cell line (DU 145, SK-MEL-28, and MES-SA/DX) and one non-tumor cell line type (MRC-5) after 72 h of exposure to 22-HTG using Alamar blue assay.

	IC_{50} μM (confidence intervals)[a]	
Cell lines	22-HTG	Doxorubicin[b]
DU 145	6.94 (6.67–7.38)	0.39 (0.32–0.48)
SK-MEL-28	3.2 (3.05–3.37)	0.22 (0.05–0.88)
MES-SA/DX	8.02 (7.6–8.79)	0.42 (0.20–0.87)
MRC5	2.61 (2.29–2.95)	0.14 (0.10–0.17)

[a] Data are presented as half-maximal inhibitory concentration (IC_{50}) value and 95% confidence intervals (CI95%) from three independent experiments performed in triplicate.
[b] Doxorubicin was used as the positive control.

overcome multidrug resistance mechanisms or act by a different pathway other than related to doxorubicin-resistance mechanism. Further studies should be perform to elucidate the proper mechanism. Cytotoxicity of 22-HTG was also evaluated in non-cancerous cells (MRC-5), and showed low selectivity. Doxorubicin, an effective chemotherapeutic anticancer drug, exhibited higher cytotoxicity to non-cancer cells than 22-HTG.

The lowest IC_{50} value for 22-HTG in cancer cells was in SK-MEL-28 (3.2 μM). This *in vitro* melanoma model presents a high resistance to the most targeted anticancer therapies due to genetic alterations, such as loss of function of p53 and PTEN, overexpression of cyclin D1, hyperactivation of NF-κB, and downregulation of p21/Cip1 (Daveri et al., 2015). Sk-Mel-28 human melanoma cells is a relevant clinical study model for the research of drugs for this type of cancer (Rossi et al., 2018) and was used for the subsequent experiments in this study.

According to the IC_{50} value in SK-MEL-28 cells, the concentrations 2.5 and 5.0 μM were defined to evaluate the effect of 22-HTG on cell viability of SK-MEL-28 cells using trypan blue staining. Exposure for 24 h with 2.5 and 5.0 μM of 22-HTG caused a significant decrease ($p < 0.05$) in the number of viable cells (Fig. 1-C).

3.2. Cell cycle analysis

Cell cycle arrest analysis was performed to evaluate whether the treatment with 22-HTG caused changes in the cell cycle progression. The cellular distribution in different phases of the cell cycle was illustrated in relation to the intracellular DNA content. As shown in Fig. 1-(D), after 24 h of treatment with 22-HTG, both concentrations decreased the number of cells in the G0/G1 and induced a significant accumulation of cells in the sub-G1 phase ($p < 0.05$), which is considered an important effect in the control of tumor growth. Treatment with doxorubicin (5.0 μM) increased the percentage of cells in the G2/M phase and reduced cells in G0/G1 and S phase.

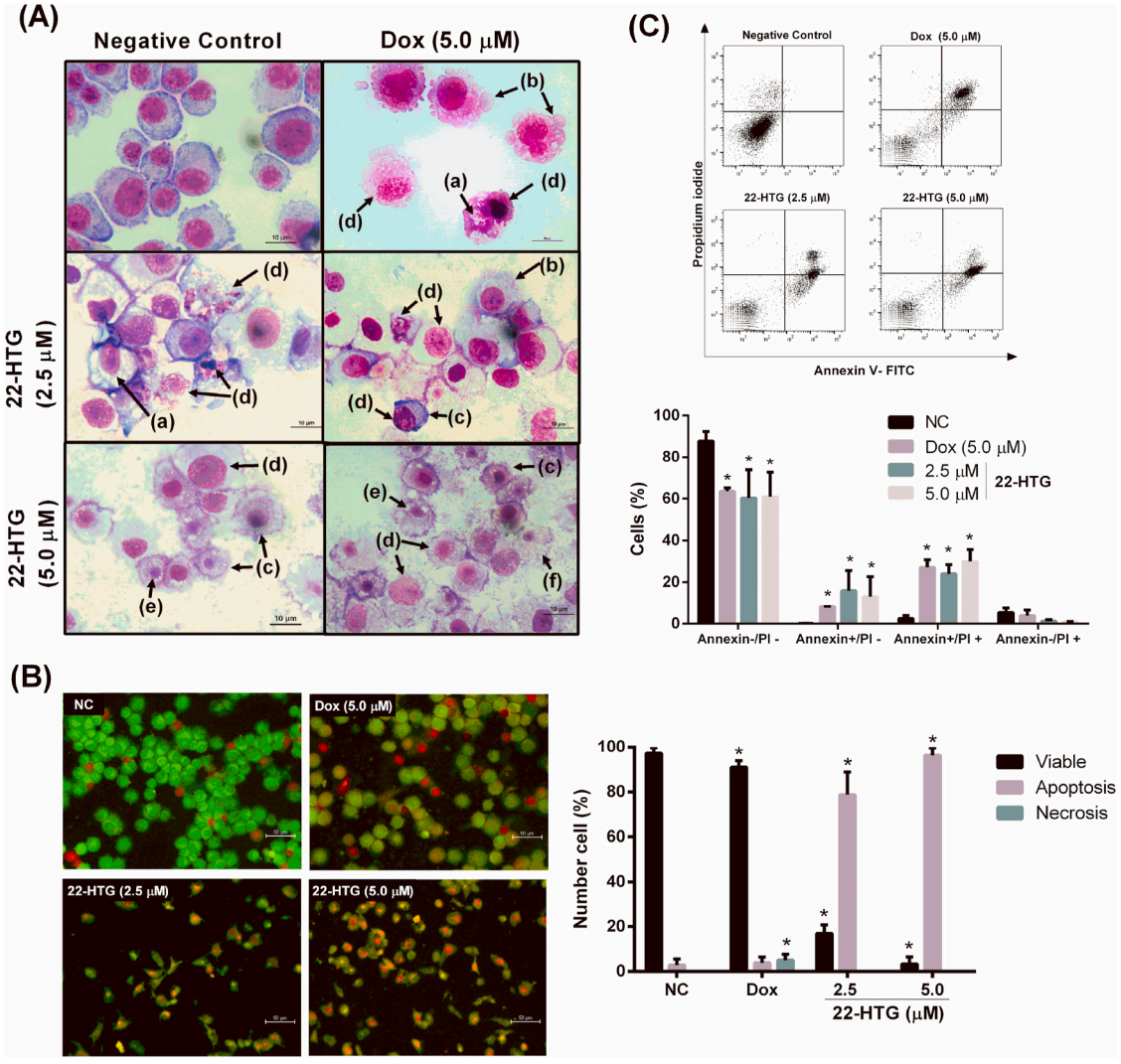

Fig. 2. Induction of apoptosis by 22β-hydroxytingenone (22-HTG). (A) Morphological changes in SK-MEL-28 cells after exposure to 22-HTG (2.5 and 5.0 μM-in duplicate) for 24 h using the rapid panoptic dye. The images demonstrate (a) intracellular vacuole, (b) plasma membrane irregularities, (c) cell retraction, (d) condensation and nuclear fragmentation, (e) cell volume reduction, and (f) instability of the plasma membrane, at a magnification of 1000x. (B) Detection of apoptosis using Aridine Orange/Ethidium bromide staining in SK-MEL-28 cells. After 24 h of treatment with 22-HTG, cells were analyzed using fluorescence microscopic as green (viable cells), green and red arrows (apoptotic cells), and red (necrotic cells). (C) 22-HTG increased apoptotic cells in human melanoma cells. Percentage of apoptotic cells after 24 h treatment with 22-HTG corresponding to viable and non-apoptotic (Annexin-/PI-), early apoptotic (Annexin+/PI-), late apoptotic (Annexin+/PI+) and necrosis cells (Annexin-/PI+). Results are expressed as mean ± SD of three independent experiments. *$p < 0.05$ was considered significant when compared to the negative control (NC). PI- Propidium iodide. Dox- Doxorubicin (5.0 μM) was used as the positive control. (For interpretation of the references to colour in this figure legend, the reader is referred to the Web version of this article.)

3.3. 22-HTG induces apoptosis in SK-MEL-28 cells

Initially, signs of apoptosis were investigated through analysis of cell morphology. Treatment with 22-HTG caused changes in the morphology of SK-MEL-28 cells, when compared to negative control group cells. The main morphological changes found in SK-MEL-28 cells after treatment with 22-HTG were condensation and nuclear fragmentation. It is also possible to observe a reduction in the cell and nucleus volume, intracellular vacuole, irregularities, and instability of the plasma membrane (Fig. 2-A). The positive control doxorubicin (5.0 μM) reduced the number of cells, induced chromatin condensation, and nuclear fragmentation and blebbing of the plasmatic membrane. The morphologic changes described suggest cell death by apoptosis and reflect the cytotoxic potential of 22-HTG in SK-MEL-28 cell line.

Apoptosis was evaluated through staining with AO/EB. Acridine orange is a vital dye that will stain both living and dead cells, whereas EB will stain only those cells that have lost their membrane integrity. Living cells turn green and can thus be distinguished from apoptotic cells (Kasibhatla, 2006). After treatment with 22-HTG, a significant decrease ($p < 0.05$) was detected in the viability of SK-MEL-28 cells, and the number of green and red-stained (apoptotic) cells increased ($p < 0.05$) in both concentrations tested (Fig. 2-B). Red-stained cells were only observed in the doxorubicin treatment. Thus, these results indicate that cell death after treatment with 22-HTG occurred through apoptosis.

Apoptotic cells were also confirmed with annexin V-FITC and PI using flow cytometry. Phosphatidylserine is a phospholipid that is presented in the cell membrane, and is normally localized on the internal surface. During the apoptosis process, this lipid is externalized and available for detection by the Annexin V-FITC conjugate, which is considered a marker of apoptosis cell death (Tischlerova et al., 2017). The use of PI in this assay allowed us to evaluate the necrotic cells, since this cellular process is characterized by the loss of membrane integrity (Amaral-Machado et al., 2019). 22-HTG induced a significant increase ($p < 0.05$) in apoptotic cell populations in early apoptosis (AnnexinV-positive/PI-negative) and late apoptosis (Annexin V-positive/PI--positive), when compared with the negative control (Fig. 2-C). Doxorubicin (5.0 μM) also induced apoptosis ($p < 0.05$).

End-stage apoptosis is characterized by loss of the plasma membrane integrity, and this is also possible to observe in the necrotic phenotype (Galluzzi et al., 2018). Treatment with 22-HTG did not induce an increase in necrotic cells in AO/EB and Annexin/PI assays. Therefore, when taken together, these results suggest that 22-HTG is able to induce apoptosis in SK-MEL-28 cells.

3.4. Evaluation of mitochondrial membrane potential

Mitochondria is an important cellular organelle and changes in the mitochondrial membrane potential and permeability are indicators of mitochondrial dysfunction, and result in apoptosis induction (Amaral-Machado et al., 2019; Tischlerova et al., 2017).

Integrity or disruption of the mitochondrial membrane potential can be detected using rhodamine 123, a green-fluorescent dye stored in active mitochondria. A decrease in mitochondrial membrane potential is indicated by a reduction in fluorescence intensity (Rodrigues et al., 2018). Treatment with 22-HTG caused significant ($p < 0.05$) mitochondrial membrane potential loss in the SK-MEL-28 cells, and showed that 22-HTG induced mitochondrial damage (Fig. 3). The positive control, doxorubicin (5.0 μM), also caused significant mitochondrial damage.

3.5. Evaluation of intracellular ROS levels

DCFH-DA is a specific ROS indicator (Chen et al., 2015) and was used to investigate whether 22-HTG causes increased intracellular ROS levels, which would be linked to its cytotoxic effect. Fig. 4 shown a reduction in the number of positive DCF-DA cells after treatment with

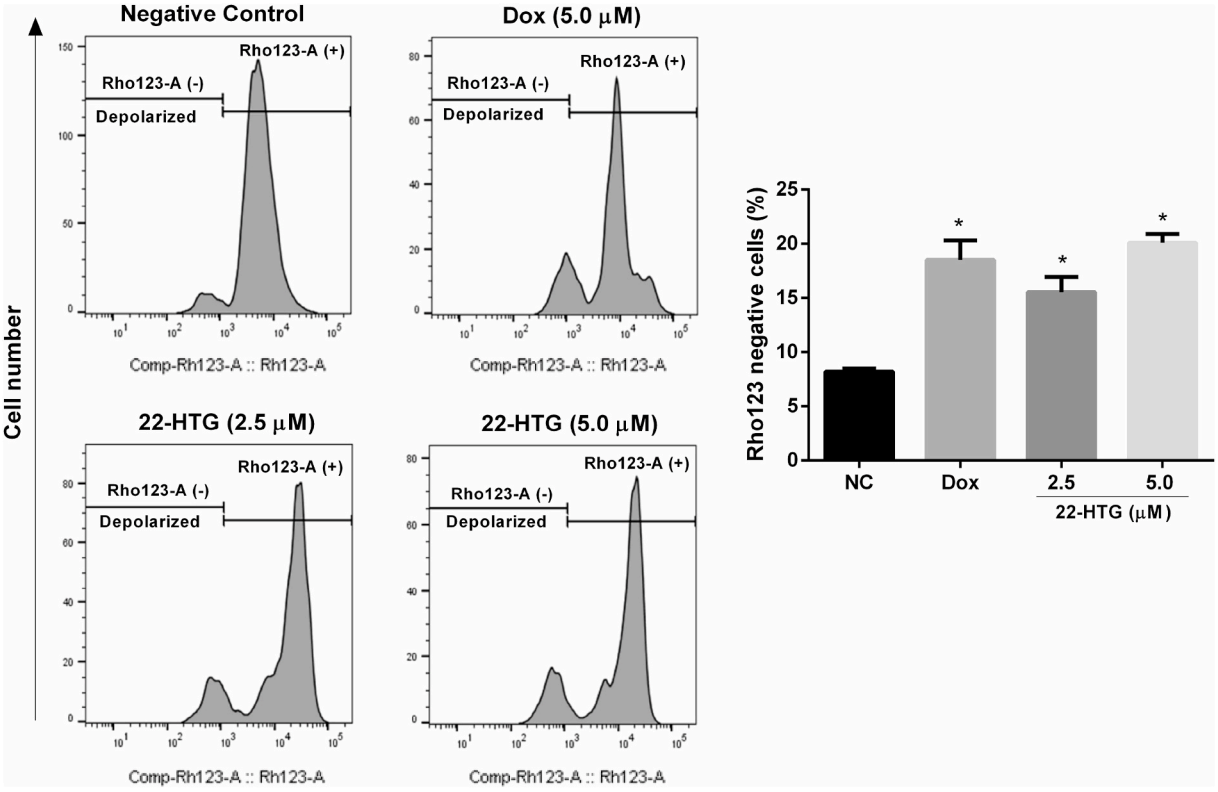

Fig. 3. Mitochondrial membrane potential of SK-MEL-28 cells using rhodamine123 after 24 h of treatment with 22-HTG. Results are expressed as mean ± SD of three independent experiments. *$p < 0.05$ was considered significant when compared to the negative control (NC). Rho123- Rhodamine 123. Dox- Doxorubicin (5.0 μM) was used as the positive control.

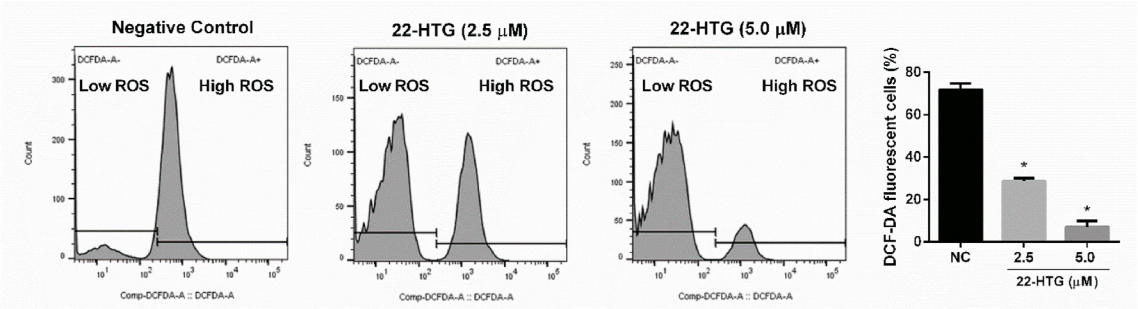

Fig. 4. Detection of intracellular Reactive Oxygen Species (ROS) level in SK-MEL-28 cells after 3 h of treatment with 22-HTG. ROS level was observed using DCFH-DA fluorescence staining procedure through flow cytometry. Results are expressed as mean ± SD of three independent experiments. *p < 0.05 was considered significant when compared to the negative control (NC).

22-HTG, and reveals that exposure to 22-HTG (2.5 and 5.0 μM) significantly decreased ($p < 0.05$) the production of ROS in SK-MEL-28 cells.

3.6. mRNA isolation and expression analysis using RT-qPCR

We also investigated whether 22-HTG affects *BRAF*, *NRAS*, and *KRAS* gene expression, which are important biomarkers in melanoma due to their involvement in the MAPK signaling pathway, and described in approximately 90% of cases of melanoma (Strickland et al., 2015). The results showed that the transcript levels of all the genes evaluated were significantly reduced by the treatment with 22HTG (2.5 μM) after 24h of exposure when compared with the negative control ($p < 0.05$), as shown in Fig. 5.

3.7. Invasion decreases after 22-HTG treatment in 3D models

We used a reconstructed skin model with SK-MEL-28 cells, which is a more similar model to the *in vivo* 3D tumor environment, in order to test the effects of 22-HTG. As shown Fig. 6 (A-*arrow*), untreated skin reconstructions were marked by melanoma invasion and/or migration, and showed a delimited tumor area, with melanoma cells in the dermis-epidermis junction toward the dermis, which characterizes the invasion process. After 22-HTG treatment (5.0 μM), the reconstructed skin with SK-MEL-28 cells presented a decrease in invasion points (Fig. 6 A-*arrow*). Furthermore, using the reconstructed skin model, 22-HTG (5.0 μM) significantly decreased MMP-9 activity (latent and active form), however for MMP-2 reductions did not occur (Fig. 6-B).

The reduction of MMM-9 activity is in accordance with the findings of the 2D experiments (Aranha et al., 2020). It is possible that reduction of MMP-9 activity after exposure to 22-HTG may be involved in the reduction of the invasion observed in the histological analysis of reconstructed skin model with SK-MEL-28 cells.

4. Discussion

Natural products represent a source for drug discovery, since compounds isolated from medicinal plants with cytotoxic properties are important in order to identify new drugs with anticancer potential (Ahmed and Halaweish, 2014; Rodrigues et al., 2019). Recents studies have identified the cytotoxic potential of *S. impressifoia* and this effect was associated with quinonemethide triterpenes (Rodrigues et al., 2019), which are considered potent anticancer agents, since they inhibit proliferation, angiogenesis, metastasis, and cause apoptosis or autophagy in tumor cells (Salvador et al., 2017), and are thus of clinical interest (Sachan et al., 2018).

Quinonemethide triterpenes is a class of triterpenoids, which are versatile natural products against melanoma cells, in special celastrol that efficiently inhibit ATF2 transcriptional activities, activate JNK, and increase c-Jun transcriptional activities (Abbas et al., 2007). Moreover, another quinonemethide named pristimerin, attenuates cell proliferation of uveal melanoma cells by inhibiting insulin-like growth factor-1 receptor (Xie et al., 2019). Studies by our research group have reported the role of 22-HTG against melanoma cells (Aranha et al., 2020), but the mechanism that leads to its potent cytotoxic effect needs further elucidation. In the current study, we identified the anti-melanoma potential of 22-HTG through induction of apoptosis, a reduction in invasiveness of SK-MEL-28 cells in the 3D model, and interference with the MAPK signaling.

Cell proliferation may be regulated by the control of the cell cycle and apoptosis (Bi et al., 2018). The loss of normal cell cycle control is an

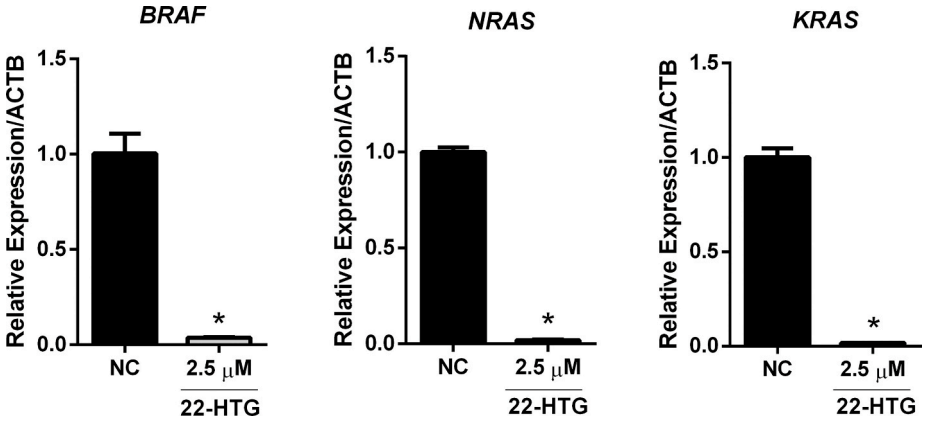

Fig. 5. Genic expression *in vitro* in SK-MEL-28 cells. Expression relative of *BRAF, NRAS,* and *KRAS* genes in SK-MEL-28 cell line after treatment with 22-HTG (2.5 μM) at 24 h. Relative expression was calculated according to the $2^{-\Delta\Delta Ct}$ method and the actin beta (ACTB) gene was used as the internal control. Results are expressed as the mean ± SD of three independent experiments. *p < 0.05 was considered significant when compared to the negative control (NC).

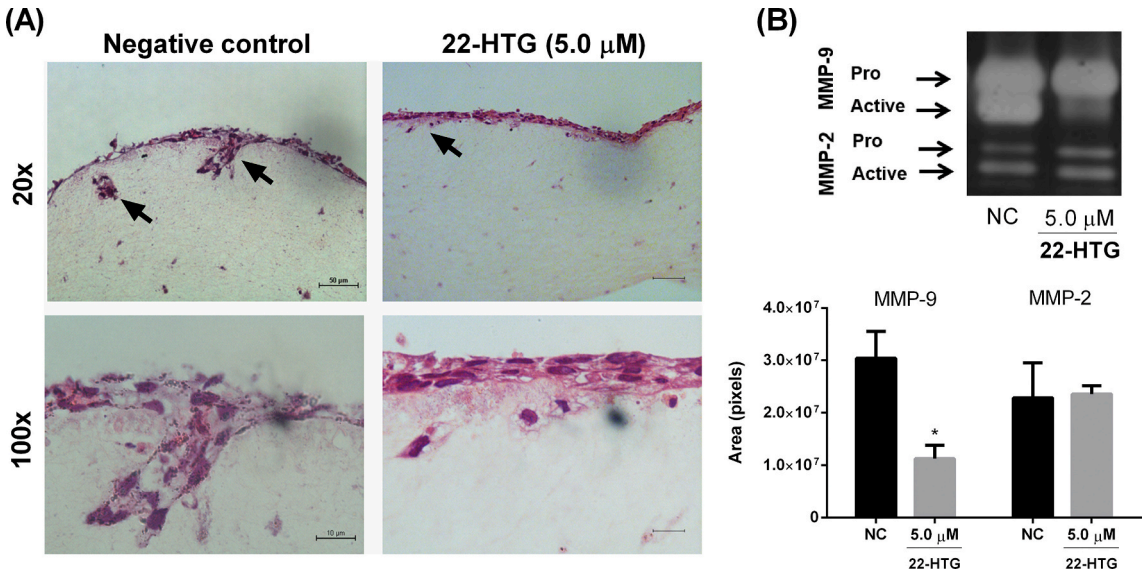

Fig. 6. Decreased invasive potential of SK-MEL-28 cells induced by 22β-hydroxytingenone (22-HTG) using 3D model. (A) Reconstructed skin with SK-MEL-28 melanoma cells untreated and treated with 22-HTG (5.0 μM) for 72 h. The images shown hematoxylin/eosin staining (20x and 100x magnification). (B) Proteolytic action of MMP-2 and MMP-9 using reconstructed skin model with SK-MEL-28 melanoma cells after treatment with 22-HTG (5.0 μM). The activity of the enzymes appeared through the light bands, indicating degradation of the substrate. Results are expressed as the mean ± SD of three independent experiments. *$p < 0.05$ was considered significant when compared to the negative control (NC).

important feature of cancer and is one which may induce uncontrolled proliferation (Menezes et al., 2018). Likewise, the sub-G1 phase of the cell cycle is a typical marker of DNA fragmentation observed in the late event of the apoptosis pathway (Beberok et al., 2019). In our study, we found that, in addition to the cytotoxic effect, 22-HTG induced morphological changes and a sub-G1 peak in cell cycle analysis. Thus, these results indicate that the antiproliferation effects were mediated by apoptosis.

Apoptosis is an important mechanism in anticancer drug research for the discovery and development of new therapeutic agents (An et al., 2019). Previous studies have shown that 22-HTG induces apoptosis in cancer stem cells in breast cancer (Cevatemre et al., 2016). In the current study, we also demonstrated that 22-HTG induced apoptosis in SK-MEL-28 cells. Several studies using quinonemethide triterpene, such as celastrol, have shown induction of apoptosis in human myeloma (Tozawa et al., 2011), breast (Mi et al., 2014), and pancreatic cancer cells (Zhao et al., 2014). Pristimerin, another quinonemethide triterpene, has shown induction of apoptosis in breast (Lee et al., 2013), prostate (Liu et al., 2014), and pancreatic cancer cells (Deeb et al., 2014). These results corroborate the findings in the present study and reinforce the idea that 22-HTG induces apoptotic-like cell death in SK-MEL-28 cells.

After verifying the events of apoptosis caused by the treatment with 22-HTG, we investigated whether this process occurs through disruption of mitochondrial membrane potential, which is a hallmark of apoptosis (Beberok et al., 2017). In cancer cells, mitochondrial damage may be a promising strategy in the regulation of apoptosis (Sharma et al., 2017). Cevatemre et al. (2016) showed that 22-HTG induced a decrease in the mitochondrial membrane potential in cancer stem cells in breast cancer. These findings suggest that mitochondrial dysfunction is possible, with induction of apoptosis via the intrinsic pathway after treatment with 22-HTG.

Several studies in the literature have shown that the cytotoxic effect of anticancer substances is caused by the intracellular increase of ROS, resulting in oxidative damage and consequently induction of apoptosis (Cho et al., 2018; Lee et al., 2019; Wang et al., 2018; Zhang et al., 2015). However, in this study we show that apoptosis induced by 22-HTG was not directly associated with ROS production in melanoma cells. A similar effect has been demonstrated using pristimerin (Wu et al., 2005), where the authors demonstrated that pristimerin did not enhance the generation of ROS. Among other findings, Wu et al. (2005) showed that pristimerin was able to induce cytochrome *c* release from isolated mitochondrial fractions in a cell-free system, and indicated the induction of mitochondrial membrane permeabilization via direct action on mitochondria.

In melanoma, there is high tumoral heterogeneity, which leads to phenotypic plasticity to support melanoma progression and resistance to drug exposure in treatment (Arozarena and Wellbrock, 2019). In the current study, 22-HTG induced apoptosis and reduced invasion of the population of melanomas with the genetic profile of SK-MEL-28 cells, and showed significant inhibition of MAPK signalling. SK-MEL-28 cells have genetic alterations, such as B-Raf^{V600E}, TP53^{R273H} and PTEN, which notoriously confer them a immense resistance to most anticancer therapies (Daveri et al., 2015; Ralph et al., 2016).

The MAPK pathway is involved in the regulation of important cellular functions, such as cell cycle control, proliferation, survival, migration, and programmed cell death (Abd El Maksoud et al., 2019; Shao et al., 2018) and, as such, play an important role in the advancement and progression of melanoma (Cicenas et al., 2017). Inhibition of the MAPK pathway has been demonstrated as an inducer of apoptosis, and causes inhibition of tumor growth (Ahmed and Halaweish, 2014). BRAF and NRAS are proteins involved with MAPK signaling pathway (Dumaz et al., 2019), which, when coupled to other mutations, are involved with the resistance mechanism, and one of the major obstacles in melanoma treatment (de Sousa et al., 2019). In this study, we have demonstrated that 22-HTG was able to inhibit genic expression of *BRAF*, *NRAS,* and *KRAS*.

In current study, using 3D human skin reconstruct model, we also demonstrated that 22-HTG decreased invasion of melanoma cells into the dermis and reduced the action of MMP-9. The 3D model is an ideal model for dissecting each step of melanoma development and progression (Li et al., 2015). Previous studies have shown that 22-HTG reduced migration, invasion, and MMP activity in 2D models (Aranha et al., 2020), which is in accordance with what was demonstrated in this study and reflects the antimetastatic potential of 22-HTG.

5. Conclusion

22β-hydroxytingenone has anti-tumorigenic properties in melanoma cells including the inhibition of proliferation, apoptosis induction, and inhibition of invasiveness potential. The MAPK pathway might also be involved, with inhibition of *BRAF*, *NRAS*, and *KRAS* genes.. Our results showed that 22β-hydroxytingenone has anticancer potential and this information could be used to support new investigations intended to study a natural product with anti-melanoma action.

Author contributions

Elenn Suzany Pereira Aranha: Conceptualization, Methodology, Formal analysis, Writing - Original Draft; **Adrhyann Jullyanne de Sousa Portilho:** Methodology, Formal analysis; **Leilane Bentes de Sousa:** Methodology, Formal analysis; **Emerson Lucena da Silva:** Methodology, Formal analysis; **Felipe Pantoja Mesquita:** Methodology, Formal analysis; **Felipe Moura Araújo da Silva:** Methodology, Formal analysis; **Waldireny C. Rocha:** Methodology, Formal analysis; **Emerson Silva Lima:** Resources; **Ana Paula Negreiros Nunes Alves:** Methodology, Formal analysis; **Hector Henrique Ferreira Koolen:** Formal analysis, Resources, Writing - Review & Editing; **Raquel Carvalho Montenegro:** Conceptualization, Resources, Writing - Review & Editing; **Marne Carvalho de Vasconcellos:** Conceptualization, Resources, Writing - Review & Editing, Funding acquisition.

Declaration of competing interest

The authors declare that there are no conflicts of interest.

Acknowledgment

This study was financed in part by the Coordenação de Aperfeiçoamento de Pessoal de Nível Superior - Brasil (CAPES) - Finance Code 001 and Fundação de Amparo à Pesquisa do Estado do Amazonas (FAPEAM, process N.030/2013) for financial support. The authors also wish to thank Sylvia Stuch-Engler from the School of Pharmaceutical Sciences, University of Sao Paulo, for generously supplying SK-MEL-28 and the Multi-User Facility of Drug Research and Development Center of the Federal University of Ceara for technical support.

References

Abbas, S., Bhoumik, A., Dahl, R., Vasile, S., Krajewski, S., Cosford, N.D.P., Ronai, Z.A., 2007. Preclinical studies of celastrol and acetyl isogambogic acid in melanoma. Clin. Canc. Res. 13, 6769–6778. https://doi.org/10.1158/1078-0432.CCR-07-1536.

Abd El Maksoud, A.I., Taher, R.F., Gaara, A.H., Abdelrazik, E., Keshk, O.S., Elawdan, K. A., Morsy, S.E., Salah, A., Khalil, H., 2019. Selective regulation of B-Raf dependent K-Ras/Mitogen-Activated Protein by natural occurring multi-kinase inhibitors in cancer cells. Front Oncol 9, 1–12. https://doi.org/10.3389/fonc.2019.01220.

Ahmed, M.S., Halaweish, F.T., 2014. Cucurbitacins: potential candidates targeting mitogen-activated protein kinase pathway for treatment of melanoma. J. Enzym. Inhib. Med. Chem. 29, 162–167. https://doi.org/10.3109/14756366.2012.762646.

Amaral-Machado, L., Oliveira, W.N., Alencar, É.N., Katarina, A., Cruz, M., Alexandre, H., Rocha, O., Ebeid, K., Salem, A.K., Sócrates, E., Egito, T., 2019. Bullfrog oil (*Rana catesbeiana* Shaw) induces apoptosis, in A2058 human melanoma cells by mitochondrial dysfunction triggered by oxidative stress. Biomed. Pharmacother. 117 https://doi.org/10.1016/j.biopha.2019.109103, 109–103.

An, W., Lai, H., Zhang, Y., Liu, M., Lin, X., Cao, S., 2019. Apoptotic pathway as the therapeutic target for anticancer traditional Chinese medicines. Front. Pharmacol. 10, 1–25. https://doi.org/10.3389/fphar.2019.00758.

Ansar Ahmed, S., Gogal, R.M., Walsh, J.E., 1994. A new rapid and simple non-radioactive assay to monitor and determine the proliferation of lymphocytes: an alternative to [3H]thymidine incorporation assay. J. Immunol. Methods 170, 211–224. https://doi.org/10.1016/0022-1759(94)90396-4.

Aranha, E.S.P., da Silva, E.L., Mesquita, F.P., de Sousa, L.B., da Silva, F.M.A., Rocha, W. C., Lima, E.S., Koolen, H.H.F., de Moraes, M.E.A., Montenegro, R.C., de Vasconcellos, M.C., 2020. 22β-hydroxytingenone reduces proliferation and invasion of human melanoma cells. Toxicol. Vitro 66, 104879. https://doi.org/10.1016/j.tiv.2020.104879.

Arozarena, I., Wellbrock, C., 2019. Phenotype plasticity as enabler of melanoma progression and therapy resistance. Nat. Rev. Canc. 19, 377–391. https://doi.org/10.1038/s41568-019-0154-4.

Beberok, A., Wrześniok, D., Szlachta, M., Rok, J., Rzepka, Z., Respondek, M., Buszman, E., 2017. Lomefloxacin induces oxidative stress and apoptosis in COLO829 melanoma cells. Int. J. Mol. Sci. 18, 2194–2211. https://doi.org/10.3390/ijms18102194.

Beberok, A., Rzepka, Z., Respondek, M., Rok, J., Stradowski, M., Wrześniok, D., 2019. Moxifloxacin as an inducer of apoptosis in melanoma cells: a study at the cellular and molecular level. Toxicol. Vitro 55, 75–92. https://doi.org/10.1016/j.tiv.2018.12.002.

Berning, L., Scharf, L., Aplak, E., Stucki, D., von Montfort, C., Reichert, A.S., Stahl, W., Brenneisen, P., 2019. In vitro selective cytotoxicity of the dietary chalcone cardamonin (CD) on melanoma compared to healthy cells is mediated by apoptosis. PloS One 14, 1–26. https://doi.org/10.1371/journal.pone.0222267.

Bi, Y.L., Min, M., Shen, W., Liu, Y., 2018. Genistein induced anticancer effects on pancreatic cancer cell lines involves mitochondrial apoptosis, G0/G1cell cycle arrest and regulation of STAT3 signalling pathway. Phytomedicine 15, 10–16. https://doi.org/10.1016/j.phymed.2017.12.001.

Boelsma, E., Gibbs, S., Faller, C., Ponec, M., 2000. Characterization and comparison of reconstructed skin models : morphological and immunohistochemical evaluation. Acta Derm. Venereol. 80, 82–88.

Brako, L., Zarucchi, J.L., 1993. Catalogue of the Flowering Plants and Gymnosperms of Peru. Catálogo de las Angiospermas y Gimnospermas del Perú. Monographs in Systematic Botany from the Missouri Botanical Gardenpp, p. 1286.

Bustin, S.A., Benes, V., Garson, J.A., Hellemans, J., Huggett, J., Kubista, M., Mueller, R., Nolan, T., Pfaffl, M.W., Shipley, G.L., Vandesompele, J., Wittwer, C.T., 2009. The MIQE guidelines: minimum information for publication of quantitative real-time PCR experiments. Clin. Chem. 55, 611–622. https://doi.org/10.1373/clinchem.2008.112797.

Cevatemre, B., Botta, B., Mori, M., Berardozzi, S., Ingallina, C., Ulukaya, E., 2016. The plant-derived triterpenoid tingenin B is a potent anticancer agent due to its cytotoxic activity on cancer stem cells of breast cancer in vitro. Chem. Biol. Interact. 260, 248–255. https://doi.org/10.1016/j.cbi.2016.10.001.

Chen, Y., Liu, J.M., Xiong, X.X., Qiu, X.Y., Pan, F., Liu, D., Lan, S.J., Jin, S., Yu, S. Bin, Chen, X.Q., 2015. Piperlongumine selectively kills hepatocellular carcinoma cells and preferentially inhibits their invasion via ROS-ER-MAPKs-CHOP. Oncotarget 6, 6406–6421. https://doi.org/10.18632/oncotarget.3444.

Cho, H.-D., Lee, J.-H., Moon, K.-D., Park, K.-H., Lee, M.-K., Seo, K.-I., 2018. Auriculasin-induced ROS causes prostate cancer cell death via induction of apoptosis. Food Chem. Toxicol. 111, 660–669. https://doi.org/10.1016/j.fct.2017.12.007.

Cicenas, J., Tamosaitis, L., Kvederaviciute, K., Tarvydas, R., Staniute, G., Kalyan, K., Meskinyte-Kausiliene, E., Stankevicius, V., Valius, M., 2017. KRAS, NRAS and BRAF mutations in colorectal cancer and melanoma. Med. Oncol. 34, 26. https://doi.org/10.1007/s12032-016-0879-9.

Clavo, Z.M.P., Cardenas, Z.P.S., Orihuela, A.O., 2003. Plantas medicinales: usadas por mujeres nativas y mestizas en la región Ucayali. Centro para la Investigación em Sistemas Sostenibles de Producción Agropecuaria, Cali (Colombia) Centro de Investigación y Divulgación en Sistemas Sostenibles Tropicales de Producción Agropecuaria, Guanare (Venezuela).

da Silva, F.M.A., Paz, W.H.P., Vasconcelos, L.-S.F., da Silva, A.L.B., da Silva-Filho, F.A., de Almeida, R.A., de Souza, A.D.L., Pinheiro, M.L.B., Koolen, H.H.F., 2016. Chemical constituents from *Salacia impressifolia* (Miers) A. C. Smith collected at the Amazon rainforest. Biochem. Systemat. Ecol. 68, 77–80. https://doi.org/10.1016/j.bse.2016.07.004.

Daveri, E., Valacchi, G., Romagnoli, R., Maellaro, E., Maioli, E., 2015. Antiproliferative effect of rottlerin on Sk-Mel-28 melanoma cells. Evid Based Complement Alternat Med 2015, 1–9. https://doi.org/10.1155/2015/545838.

de Sousa, F.S., Nunes, E.A., Gomes, K.S., Cerchiaro, G., Lago, J.H.G., 2019. Genotoxic and cytotoxic effects of neolignans isolated from *Nectandra leucantha* (Lauraceae). Toxicol. Vitro 55, 116–123. https://doi.org/10.1016/j.tiv.2018.12.011.

Deeb, D., Gao, X., Liu, Y.B.O., Pindolia, K., Gautam, S.C., 2014. Pristimerin, a quinonemethide triterpenoid, induces apoptosis in pancreatic cancer cells through the inhibition of pro-survival Akt/NF-κB/mTOR signaling proteins and anti-apoptotic Bcl-2. Int. J. Oncol. 44, 1707–1715. https://doi.org/10.3892/ijo.2014.2325.

Dumaz, N., Jouenne, F., Delyon, J., Mourah, S., Bensussan, A., Lebbé, C., 2019. Atypical BRAF and NRAS mutations in mucosal melanoma. Cancers 11, 1133. https://doi.org/10.3390/cancers11081133.

Galluzzi, L., Vitale, I., Aaronson, S.A., Abrams, J.M., Adam, D., Agostinis, P., Alnemri, E. S., Altucci, L., Amelio, I., Andrews, D.W., Annicchiarico-Petruzzelli, M., Antonov, A. V., Arama, E., Baehrecke, E.H., Barlev, N.A., Bazan, N.G., Bernassola, F., Bertrand, M.J.M., Bianchi, K., Blagosklonny, M.V., Blomgren, K., Borner, C., Boya, P., Brenner, C., Campanella, M., Candi, E., Carmona-Gutierrez, D., Cecconi, F., Chan, F.K.M., Chandel, N.S., Cheng, E.H., Chipuk, J.E., Cidlowski, J.A., Ciechanover, A., Cohen, G.M., Conrad, M., Cubillos-Ruiz, J.R., Czabotar, P.E., D'Angiolella, V., Dawson, T.M., Dawson, V.L., De Laurenzi, V., De Maria, R., Debatin, K.M., Deberardinis, R.J., Deshmukh, M., Di Daniele, N., Di Virgilio, F., Dixit, V.M., Dixon, S.J., Duckett, C.S., Dynlacht, B.D., El-Deiry, W.S., Elrod, J.W., Fimia, G.M., Fulda, S., García-Sáez, A.J., Garg, A.D., Garrido, C., Gavathiotis, E., Golstein, P., Gottlieb, E., Green, D.R., Greene, L.A., Gronemeyer, H., Gross, A., Hajnoczky, G., Hardwick, J.M., Harris, I.S., Hengartner, M.O., Hetz, C., Ichijo, H., Jäättelä, M., Joseph, B., Jost, P.J., Juin, P.P., Kaiser, W.J., Karin, M., Kaufmann, T., Kepp, O., Kimchi, A., Kitsis, R.N., Klionsky, D.J., Knight, R.A., Kumar, S., Lee, S.W., Lemasters, J.J., Levine, B., Linkermann, A., Lipton, S.A., Lockshin, R.A., López-Otín, C., Lowe, S.W., Luedde, T., Lugli, E., MacFarlane, M., Madeo, F., Malewicz, M., Malorni, W., Manic, G., Marine, J.C., Martin, S.J., Martinou, J.C., Medema, J.P., Mehlen, P., Meier, P., Melino, S., Miao, E.A., Molkentin, J.D., Moll, U.M., Muñoz-Pinedo, C., Nagata, S., Nuñez, G., Oberst, A., Oren, M., Overholtzer, M., Pagano, M.,

Panaretakis, T., Pasparakis, M., Penninger, J.M., Pereira, D.M., Pervaiz, S., Peter, M. E., Piacentini, M., Pinton, P., Prehn, J.H.M., Puthalakath, H., Rabinovich, G.A., Rehm, M., Rizzuto, R., Rodrigues, C.M.P., Rubinsztein, D.C., Rudel, T., Ryan, K.M., Sayan, E., Scorrano, L., Shao, F., Shi, Y., Silke, J., Simon, H.U., Sistigu, A., Stockwell, B.R., Strasser, A., Szabadkai, G., Tait, S.W.G., Tang, D., Tavernarakis, N., Thorburn, A., Tsujimoto, Y., Turk, B., Vanden Berghe, T., Vandenabeele, P., Vander Heiden, M.G., Villunger, A., Virgin, H.W., Vousden, K.H., Vucic, D., Wagner, E.F., Walczak, H., Wallach, D., Wang, Y., Wells, J.A., Wood, W., Yuan, J., Zakeri, Z., Zhivotovsky, B., Zitvogel, L., Melino, G., Kroemer, G., 2018. Molecular mechanisms of cell death: recommendations of the nomenclature committee on cell death 2018. Cell Death Differ. 25, 486–541. https://doi.org/10.1038/s41418-017-0012-4.

Greer, D.A., Ivey, S., 2007. Distinct N-glycan glycosylation of P-glycoprotein isolated from the human uterine sarcoma cell line MES-SA/Dx5. Biochim. Biophys. Acta 17770, 1275–1282. https://doi.org/10.1016/j.bbagen.2007.07.005.

Guerra, A.C.V.A., Soares, L.A.L., Ferreira, M.R.A., Araújo, A.A., Rocha, H.A.O., Medeiros, J.S., Cavalcante, R.D.S., Júnior, R.F.A., 2017. *Libidibia ferrea* presents antiproliferative, apoptotic and antioxidant effects in a colorectal cancer cell line. Biomed. Pharmacother. 92, 696–706. https://doi.org/10.1016/j.biopha.2017.05.123.

Huang, L., Peng, B., Nayak, Y., Wang, C., Si, F., Liu, X., Dou, J., Xu, H., Peng, G., 2020. Baicalein and Baicalin promote melanoma apoptosis and senescence via metabolic inhibition. Front Cell Dev Biol 8, 836. https://doi.org/10.3389/fcell.2020.00836.

Kasibhatla, S., 2006. Acridine Orange/Ethidium Bromide (AO/EB) staining to detect apoptosis. Cold Spring Harb. Protoc. 2006 https://doi.org/10.1101/pdb.prot4493 pdb.prot4493-pdb.prot4493.

Kozar, I., Margue, C., Rothengatter, S., Haan, C., Kreis, S., 2019. Many ways to resistance: how melanoma cells evade targeted therapies. Biochim. Biophys. Acta Rev. Canc 1871, 313–322. https://doi.org/10.1016/j.bbcan.2019.02.002.

Lee, J.S., Yoon, I.S., Lee, M.S., Cha, E.Y., Thuong, P.T., Diep, T.T., Kim, J.R., 2013. Anticancer activity of pristimerin in epidermal growth factor receptor 2-positive SKBR3 human breast cancer cells. Biol. Pharm. Bull. 36, 316–325. https://doi.org/10.1248/bpb.b12-00685.

Lee, Y.J., Kim, W. Il, Kim, S.Y., Cho, S.W., Nam, H.S., Lee, S.H., Cho, M.K., 2019. Flavonoid morin inhibits proliferation and induces apoptosis of melanoma cells by regulating reactive oxygen species, Sp1 and Mcl-1. Arch Pharm. Res. (Seoul) 42, 531–542. https://doi.org/10.1007/s12272-019-01158-5.

Leonardi, G., Falzone, L., Salemi, R., Zanghï¿½, A., Spandidos, D., Mccubrey, J., Candido, S., Libra, M., 2018. Cutaneous melanoma: from pathogenesis to therapy (Review). Int. J. Oncol. 52, 1071–1080. https://doi.org/10.3892/ijo.2018.4287.

Li, Ling, Fukunaga-Kalabis, Mizuho, Herlyn, Meenhard, 2015. Establishing human skin grafts in mice as model for melanoma progression. Methods Mol Biol 1–11. https://doi.org/10.1007/7651_2015_301.

Liu, Y.B., Gao, X., Deeb, D., Brigolin, C., Zhang, Y., Shaw, J., Pindolia, K., Gautam, S.C., 2014. Ubiquitin-proteasomal degradation of antiapoptotic survivin facilitates induction of apoptosis in prostate cancer cells by pristimerin. Int. J. Oncol. 45, 1735–1741. https://doi.org/10.3892/ijo.2014.2561.

Lombardi, J., 2010. Notas nomenclaturais em salacioideae (Celastraceae). Rodriguesia 61, 123–125.

Lorenzi, H., Matos, F.J.A., 2002. Plantas medicinais no Brasil: Nativas e exóticas cultivadas. Instituto Plantarum, Nova Odessa.

Maria, S.S., Wada, M.L.F., 1997. Cytoquemical analysis of vero cell on type I collagen gels in long-term culture. In Vitro Cell. Dev. Biol. Anim. 33, 748–750. https://10.1007/s11626-997-0152-9.

Menezes, A.C., Carvalheiro, M., Ferreira de Oliveira, J.M.P., Ascenso, A., Oliveira, H., 2018. Cytotoxic effect of the serotonergic drug 1-(1-Naphthyl)piperazine against melanoma cells. Toxicol. Vitro 47, 72–78. https://doi.org/10.1016/j.tiv.2017.11.011.

Mi, C., Shi, H., Ma, J., Han, L.Z., Lee, J.J., Jin, X., 2014. Celastrol induces the apoptosis of breast cancer cells and inhibits their invasion via downregulation of MMP-9. Oncol. Rep. 32, 2527–2532. https://doi.org/10.3892/or.2014.3535.

Moreira, R.S., Bicker, J., Musicco, F., Persichetti, A., Pereira, A.M.P.T., 2020. Anti-PD-1 immunotherapy in advanced metastatic melanoma: state of the art and future challenges. Life Sci. 240, 117093. https://doi.org/10.1016/j.lfs.2019.117093.

Oprean, C., Ivan, A., Bojin, F., Cristea, M., Soica, C., Drăghia, L., Caunii, A., Paunescu, V., Tatu, C., 2018. Selective in vitro anti-melanoma activity of ursolic and oleanolic acids. Toxicol. Mech. Methods 28, 148–156. https://doi.org/10.1080/15376516.2017.1373881.

Pedrosa, N., Catarino, C.M., Pennacchi, P.C., 2017. A new reconstructed human epidermis for in vitro skin irritation testing. Toxicol. Vitro 42, 31–37. https://doi.org/10.1016/j.tiv.2017.03.010.

Ralph, A.C.L., Calcagno, D.Q., da Silva Souza, L.G., de Lemos, T.L.G., Montenegro, R.C., de Arruda Cardoso Smith, M., de Vasconcellos, M.C., 2016. Biflorin induces cytotoxicity by DNA interaction in genetically different human melanoma cell lines. Toxicol. Vitro 34, 237–245. https://doi.org/10.1016/j.tiv.2016.04.007.

Ribeiro, F.M., Volpato, H., Lazarin-Bidóia, D., Desoti, V.C., de Souza, R.O., Fonseca, M.J. V., Ueda-Nakamura, T., Nakamura, C.V., Silva, S. de O., 2018. The extended production of UV-induced reactive oxygen species in L929 fibroblasts is attenuated by posttreatment with *Arrabidaea chica* through scavenging mechanisms. J. Photochem. Photobiol., B 178, 175–181. https://doi.org/10.1016/j.jphotobiol.2017.11.002.

Rodrigues, M. do D., Santiago, P.B.G.S., Marques, K.M.R., Pereira, V.R.A., de Castro, M.C. A.B., Cantalice, J.C.L.L., da Silva, T.G., Adam, M.L., do Nascimento, S.C., de Albuquerque, J.F.C., Militao, G.C.G., 2018. Selective cytotoxic and genotoxic activities of 5-(2-bromo-5-methoxybenzylidene)-thiazolidine-2,4-dione against NCI-H292 human lung carcinoma cells. Pharmacol. Rep. 70, 446–454. https://doi.org/10.1016/j.pharep.2017.11.008.

Rodrigues, A.C.B.d.C., Oliveira, F.P.d., Dias, R.B., Sales, C.B.S., Rocha, C.A.G., Soares, M. B.P., Costa, E.V., Silva, F.M.A.d., Rocha, W.C., Koolen, H.H.F., Bezerra, D.P., 2019. In vitro and in vivo anti-leukemia activity of the stem bark of *Salacia impressifolia* (Miers) A. C. Smith (Celastraceae). J. Ethnopharmacol. 231, 516–524. https://doi.org/10.1016/j.jep.2018.11.008.

Rosenberg, E.E., Gerashchenko, G.V., Kashuba, V.I., 2014. Comparative analysis of gene expression in normal and cancer human prostate cell lines. Ukrainian Biochem. J. 86, 119–128. https://doi.org/10.15407/ubj86.02.119.

Rossi, S., Cordella, M., Tabolacci, C., Nassa, G., D'Arcangelo, D., Senatore, C., Pagnotto, P., Magliozzi, R., Salvati, A., Weisz, A., Facchiano, A., Facchiano, F., 2018. TNF-alpha and metalloproteases as key players in melanoma cells aggressiveness. J. Exp. Clin. Canc. Res. 37, 326. https://doi.org/10.1186/s13046-018-0982-1.

Sachan, R., Kundu, A., Jeon, Y., Choi, W.S., Yoon, K., Kim, I.S., Kwak, J.H., Kim, H.S., 2018. Afrocyclamin A, a triterpene saponin, induces apoptosis and autophagic cell death via the PI3K/Akt/mTOR pathway in human prostate cancer cells. Phytomedicine 51, 139–150. https://doi.org/10.1016/j.phymed.2018.10.012.

Salvador, J.A.R., Leal, A.S., Valdeira, A.S., Gonçalves, B.M.F., Alho, D.P.S., Figueiredo, S. A.C., Silvestre, S.M., Mendes, V.I.S., 2017. Oleanane-, ursane-, and quinone methide friedelane-type triterpenoid derivatives: recent advances in cancer treatment. Eur. J. Med. Chem. 142, 95–130. https://doi.org/10.1016/j.ejmech.2017.07.013.

Savoia, P., Fava, P., Casoni, F., Cremona, O., 2019. Targeting the ERK signaling pathway in melanoma. Int. J. Mol. Sci. 20, 1483. https://doi.org/10.3390/ijms20061483.

Schmittgen, T.D., Livak, K.J., 2008. Analyzing real-time PCR data by the comparative CT method. Nat. Protoc. 3, 1101–1108. https://doi.org/10.1038/nprot.2008.73.

Shao, W., Mishina, Y.M., Feng, Y., Caponigro, G., Cooke, V.G., Rivera, S., Wang, Y., Shen, F., Korn, J.M., Mathews Griner, L.A., Nishiguchi, G., Rico, A., Tellew, J., Haling, J.R., Aversa, R., Polyakov, V., Zang, R., Hekmat-Nejad, M., Amiri, P., Singh, M., Keen, N., Dillon, M.P., Lees, E., Ramurthy, S., Sellers, W.R., Stuart, D.D., 2018. Antitumor properties of RAF709, a highly selective and potent inhibitor of RAF kinase dimers, in tumors driven by mutant RAS or BRAF. Canc. Res. 78, 1537–1548. https://doi.org/10.1158/0008-5472.CAN-17-2033.

Sharma, G., Rana, N.K., Singh, P., Dubey, P., Pandey, D.S., Koch, B., 2017. P53 dependent apoptosis and cell cycle delay induced by heteroleptic complexes in human cervical cancer cells. Biomed. Pharmacother. 88, 218–231. https://doi.org/10.1016/j.biopha.2017.01.044.

Strickland, L.R., Pal, H.C., Elmets, C.A., Afaq, F., 2015. Targeting drivers of melanoma with synthetic small molecules and phytochemicals. Canc. Lett. 359, 20–35. https://doi.org/10.1016/j.canlet.2015.01.016.

Strober, W., 2001. Trypan blue exclusion test of cell viability. In: Current Protocols in Immunology. John Wiley & Sons, Inc., Hoboken, NJ, USA https://doi.org/10.1002/0471142735.ima03bs21. Appendix 3B.

Tischlerova, V., Kello, M., Mojzis, J., Budovska, M., 2017. Indole phytoalexin derivatives induce mitochondrial mediated apoptosis in human colorectal carcinoma cells. World J. Gastroenterol. 23, 4341–4353. https://doi.org/10.3748/wjg.v23.i24.4341.

Tozawa, K., Sagawa, M., Kizaki, M., 2011. Quinone methide tripterine, celastrol, induces apoptosis in human myeloma cells via NF-Bκ pathway. Int. J. Oncol. 39, 1117–1122. https://doi.org/10.3892/ijo.2011.1161.

Vartholomatos, G., Alexiou, G.A., Stefanaki, K., Lykoudis, E.G., Tseka, G., Tzoufi, M., Sfakianos, G., Prodromou, N., 2015. The value of cell cycle analysis by propidium-iodine staining of CD56+ cells in pediatric brain tumors. Clin. Neurol. Neurosurg. 133, 70–74. https://doi.org/10.1016/j.clineuro.2015.03.017.

Wang, S., Hu, Y., Yan, Y., Cheng, Z., Liu, T., 2018. Sotetsuflavone inhibits proliferation and induces apoptosis of A549 cells through ROS-mediated mitochondrial-dependent pathway. BMC Compl. Alternative Med. 18, 1–11. https://doi.org/10.1186/s12906-018-2300-z.

Wu, C.C., Chan, M.L., Chen, W.Y., Tsai, C.Y., Chang, F.R., Wu, Y.C., 2005. Pristimerin induces caspase-dependent apoptosis in MDA-MB-231 cells via direct effects on mitochondria. Mol. Canc. Therapeut. 4, 1277–1285. https://doi.org/10.1158/1535-7163.MCT-05-0027.

Xie, X., Xie, S., Xie, C., Fang, Y., Li, Z., Wang, R., Jiang, W., 2019. Pristimerin attenuates cell proliferation of uveal melanoma cells by inhibiting insulin-like growth factor-1 receptor and its downstream pathways. J. Cell Mol. Med. 23, 7545–7553. https://doi.org/10.1111/jcmm.14623.

Zhang, C., Jia, X., Bao, J., Chen, S., Wang, K., Zhang, Y., Li, P., Wan, J.-B., Su, H., Wang, Y., Mei, Z., He, C., 2015. Polyphyllin VII induces apoptosis in HepG2 cells through ROS-mediated mitochondrial dysfunction and MAPK pathways. BMC Compl. Alternative Med. 16, 58. https://doi.org/10.1186/s12906-016-1036-x.

Zhao, X., Gao, S., Ren, H., Huang, H., Ji, W., Hao, J., 2014. Inhibition of autophagy strengthens celastrol-induced apoptosis in human pancreatic cancer in vitro and in vivo models. Curr. Mol. Med. 14, 555–563. https://doi.org/10.2174/1566524014666140414211223.